

# ARBITRARILY HIGH-ORDER CONSERVATIVE SCHEMES FOR THE GENERALIZED KORTEWEG-DE VRIES EQUATION

KAI YANG

**ABSTRACT.** This paper proposes a new class of arbitrarily high-order conservative numerical schemes for the generalized Korteweg-de Vries (KdV) equation. This approach is based on the scalar auxiliary variable (SAV) method. The equation is reformulated into an equivalent system by introducing a scalar auxiliary variable, and the energy is reformulated into a sum of two quadratic terms. Therefore, the quadratic preserving Runge-Kutta method will preserve both the mass and the reformulated energy in the discrete time flow. With the Fourier pseudo-spectral spatial discretization, the scheme conserves the first and third invariant quantities (momentum and energy) exactly in the fully discrete sense. The discrete mass possesses the precision of the spectral accuracy.

## 1. INTRODUCTION

This paper considers the numerical approximation of the generalized Korteweg-de Vries (gKdV) equation

$$(1.1) \quad \begin{cases} u_t = -(u_{xx} + \frac{1}{p}u^p)_x, & x \in \mathbb{R}, t > 0 \\ u(x, 0) = u_0, \end{cases}$$

where  $p$  is a positive integer.

When  $p = 2$ , it is known as the KdV equation, which was first studied numerically in [71], long after John Scott Russell's experimental observation in 1834. When  $p = 3$ , it is the modified KdV (mKdV) equation. One appealing feature of these two cases is that they form the integrable systems and possess infinitely many integrals, which are invariant in time, see [55]. This is accounted by reformulating the KdV equation into the Lax pairs [42]. When  $p \geq 4$ , it is known as the generalized KdV equation, which is not integrable. In general, the equation (1.1) conserves the following three invariant quantities:

$$(1.2) \quad I[u(t)] \stackrel{\text{def}}{=} \int u(x, t) dx = I[u_0];$$

$$(1.3) \quad M[u(t)] \stackrel{\text{def}}{=} \int [u(x, t)]^2 dx = M[u_0];$$

$$(1.4) \quad E[u(t)] \stackrel{\text{def}}{=} \int \left[ \frac{1}{2} (u_x(x, t))^2 - \frac{1}{p(p+1)} (u(x, t))^{p+1} \right] dx = E[u_0],$$

---

*Date:* December 24, 2024.

*Key words and phrases.* generalized KdV, SAV, energy conservation, high-order conservative scheme.

known as the momentum, mass and energy (Hamiltonian), respectively.

These evolution equations are among the simplest of a general class of models featuring nonlinear convection (the term  $(\frac{1}{p}u^p)_x$  in this case). This family of equations arise as mathematical models for the propagation of physical waves in a wide variety of situations, such as shallow-water waves with weakly non-linear restoring forces, long internal waves in a density-stratified ocean, ion-acoustic waves in a plasma, acoustic waves on a crystal lattice, etc., e.g., see [6], [35], [59], [10], [9], [1], [13], [20], [58], [11], [2]. The equations also attracted attention from the mathematical theory side. Analytical and numerical investigations include well-posedness, [38], [39]; soliton stability, [14], [49]; dispersion limit, [28], [29]; and singularity formations, [50], [52], [54], [53], [41]. Nevertheless, there are still many open questions, and therefore, an efficient and accurate numerical algorithm would be desirable for future investigations.

Numerical studies of the gKdV equation trace back to 1970's, ranging from finite difference methods [26], [30], [43], [22], [66]; finite element methods [4], [67], [3], [5], [23], [12], [8], [36]; spectral methods [24], [31], [34], [47], [48], [60]; operator splitting methods [33], [32] and discontinuous Galerkin methods [17], [44], [68], [69], [7], [70], [45]. Besides the order of accuracy and the stiffness from the term  $u_{xxx}$ , preserving the conservation laws (1.2)-(1.4) is also a main concern in designing a numerical method for (1.1). Indeed, for conservative PDEs, numerical methods, which can preserve the corresponding invariants, are often advantageous: besides the accuracy, a conservative scheme can preserve good stability properties, especially in long-time simulations. On the other hand, to our best knowledge, most of the papers above are only capable of preserving one or, possibly, two quantities from (1.2)-(1.4), with the second order accuracy in time.

The purpose of this paper is to present a numerical scheme for the gKdV equation that preserves all these three invariant quantities in (1.2)-(1.4) exact in the discrete time, together with an arbitrarily high order of temporal accuracy. This is achieved by applying the scalar auxiliary variable (SAV) approach. The SAV approach was proposed for minimizing the free energy by gradient flows, aiming to keep the energy stable in the numerical time flow, see [63], [62] and convergence analysis in [64]. It is then applied to the Hamiltonian PDEs in [16] and [21]. Inspired by the same idea, we reformulate the equation (1.1) into an equivalent system by introducing an auxiliary variable. The reformulated system conserves the original momentum and mass, and also the modified energy, which is rewritten into the sum of two quadratic terms. Therefore, by the standard numerical ODE theory, the quadratic preserving (symplectic) Runge-Kutta methods will preserve all these three invariants exactly in the discrete time flow. The standard Fourier pseudo-spectral method is chosen for the spatial discretization. This spatial discretization preserves the momentum and energy exactly in the fully discrete sense; the error of the discrete mass comes from the spatial discretization, which is of spectral accuracy and almost unnoticeable in our numerical experiments.

This paper is organized as follows. In Section 2, we give the equivalent form of the reformulated gKdV equation (1.1) and the modified energy (1.4) based on the SAV approach.

In Section 3, we show that the family of the quadratic preserving (symplectic) Runge-Kutta methods will preserve the momentum, mass and modified energy in the discrete time flow. In Section 4, we describe the spatial discretization. We prove that the conservation laws (1.2) and (1.4) hold in the spatial discrete sense. We also show the error of (1.3) from this discretization. Combining with results in Section 3, we prove that the proposed scheme preserves the momentum and energy exactly in the full discrete sense. In the meanwhile, we also give an upper estimate of the error for the discrete mass, which is  $\sim C_d \cdot t$  for some constant  $C_d$  coming from the error of the spatial discretization. Due to the high accuracy of the Fourier spectral method, the constant  $C_d$  is generally on the order of  $10^{-14}$ , several orders smaller than the tolerance for solving the resulting nonlinear system, and thus, the discrete mass error is almost unnoticeable. In Section 5, we first describe the numerical algorithm for solving the resulting nonlinear system from the symplectic Runge-Kutta method. This is based on the fixed point iteration similar to [21]. Then, we list our numerical examples. The earlier proposed numerical methods such as the 2nd order implicit Runge-Kutta (IRK2), the 4th order implicit Runge-Kutta (IRK4) (see, e.g., [15], [18], [56]) and the 4th order modified exponential time differencing (mETDRK4) ([19] and [37]) method are also used for a comparison. The numerical results show the fulfillment of conservation laws and a significant accuracy of the proposed scheme.

**Acknowledgement:** The author is partially supported by the NSF grant DMS-1927258 (PI: Svetlana Roudenko). The author is thankful for Dr. Roudenko's helpful discussion, reading and remarks on the paper.

## 2. MODEL REFORMULATION BY THE SAV APPROACH

In this section, we reformulate the equation (1.1) into an equivalent system, which possesses a modified energy function of a new variable.

We first define the inner product for the real valued functions  $f, g \in L^2(\mathbb{R})$  :

$$(2.1) \quad (f, g) \stackrel{\text{def}}{=} \int_{\mathbb{R}} f(x)g(x)dx.$$

Consider a new scalar variable

$$v \stackrel{\text{def}}{=} v(u, t) = \sqrt{(u^p, u) + C_0},$$

where  $C_0$  is a large enough positive constant to prevent the expression  $(u^p, u) + C_0$  under the square root to become negative during our simulation time  $t \in [0, T]$ . In Section 3, we will provide an adjustment process for  $C_0$  when  $v(t_m)$  is close to 0 at some time  $t = t_m$ . Therefore, for now we only need to choose a constant  $C_0$  at  $t = t_m$  to make sure  $v(t) > 0$  for  $t \in [t_m, t_{m+1}]$ . This can be easily achieved, since we assume that the solution is well-posed (smooth in time) in  $t \in [0, T]$ .

The equation (1.1) is then reformulated into the following system

$$(2.2) \quad \begin{cases} u_t = - \left( u_{xx} + \frac{1}{p} \frac{u^p v}{\sqrt{(u^p, u) + C_0}} \right)_x \stackrel{\text{def}}{=} f(u, v), \\ v_t = \frac{p+1}{2\sqrt{(u^p, u) + C_0}} (u^p, u_t) \stackrel{\text{def}}{=} g(u, v), \end{cases}$$

with the initial condition

$$u(x, 0) = u_0, \quad v_0 = \sqrt{(u_0^p, u_0) + C_0}.$$

Since the modified system (2.2) is identical to (1.1) at the continuous level, the modified system (2.2) conserves the momentum, mass and modified energy in the form

$$(2.3) \quad I[u(t)] \stackrel{\text{def}}{=} (u, 1) \equiv I[u_0];$$

$$(2.4) \quad M[u(t)] \stackrel{\text{def}}{=} (u, u) \equiv M[u_0];$$

$$(2.5) \quad E[u(t), v(t)] \stackrel{\text{def}}{=} -\frac{1}{2}(u_{xx}, u) - \frac{1}{p(p+1)}(v^2 - C_0) \equiv E[u_0, v_0].$$

### 3. TEMPORAL DISCRETIZATION

In this section, we describe the temporal discretization of the scheme. We first show that the family of the symplectic Runge-Kutta (SRK) methods will conserve all three quantities (2.3) (2.4) and (2.5) in the discrete time flow. Then, we propose a strategy to adjust the constant  $C_0$  in the computation, which makes the reformulated system (2.2) valid all the time and keeps the energy invariant.

**3.1. Symplectic Runge-Kutta method.** We first recall the  $s$ -stage collocation Runge-Kutta method. Consider our simulation on the time interval  $t \in [0, T]$ . Define  $\tau$  to be the time step and  $t_m = m\tau$ . Denote the semi-discretization in time  $u^m \approx u(x, t_m)$ ,  $v^m \approx v(t_m)$ . Let  $b_i$ ,  $a_{ij}$  ( $i, j = 1, \dots, s$ ) be real numbers, and  $c_i = \sum_{j=1}^s a_{ij}$  be the collocation points. Denote the intermediate values  $U_i$  and  $V_i$  to be the solution satisfying (2.2) exactly at the time  $t = t_m + \tau c_i$ . Then, for given  $u^m$  and  $v^m$ , the intermediate values  $U_i$  and  $V_i$  for the solution at  $t = t_m + \tau c_i$  are calculated by

$$(3.1) \quad U_i = u^m + \tau \sum_{j=1}^s a_{ij} f_j, \quad V_i = v^m + \tau \sum_{j=1}^s a_{ij} g_j,$$

where  $f_i = f(U_i, V_i)$  and  $g_i = g(U_i, V_i)$ . Then,  $u^{m+1}$  and  $v^{m+1}$  are updated by

$$(3.2) \quad u^{m+1} = u^m + \tau \sum_{i=1}^s b_i f_i, \quad v^{m+1} = v^m + \tau \sum_{i=1}^s b_i g_i.$$

We usually write the coefficients  $\mathbf{A} = (a_{ij})$ ,  $\mathbf{b} = (b_1, b_2, \dots, b_s)$  and  $\mathbf{c} = (c_1, c_2, \dots, c_s)^T$  in the Butcher's Tableaus ([15]):

$$\begin{array}{c|c} \mathbf{c} & \mathbf{A} \\ \hline & \mathbf{b} \end{array}.$$

For example, we list three commonly used Runge-Kutta methods in the Butcher's Tableaus in Table 1. They are the  $s$ -stage Runge-Kutta methods with  $s = 1, 2, 3$ , respectively. These are all collocation methods coming from the Gaussian-Legendre quadrature, known as the IRK2, IRK4 and IRK6 methods, since the temporal accuracy is on the order of 2, 4, 6, respectively. We use these methods in our numerical examples. There are many other types of collocation Runge-Kutta methods, we refer the interested reader to [6], [18], [56], [25] and [57].

$\begin{array}{c c} \frac{1}{2} & \frac{1}{2} \\ \hline & 1 \end{array}$	$\begin{array}{c cc} \frac{1}{2} - \frac{1}{6}\sqrt{3} & \frac{1}{4} & \frac{1}{4} - \frac{1}{6}\sqrt{3} \\ \frac{1}{2} + \frac{1}{6}\sqrt{3} & \frac{1}{4} + \frac{1}{6}\sqrt{3} & \frac{1}{4} \\ \hline & \frac{1}{2} & \frac{1}{2} \end{array}$
(A) IRK2	(B) IRK4
$\begin{array}{c cc} \frac{1}{2} - \frac{\sqrt{15}}{10} & \frac{5}{36} & \frac{2}{9} - \frac{\sqrt{15}}{15} \\ & \frac{5}{36} + \frac{\sqrt{15}}{24} & \frac{2}{9} \\ \frac{1}{2} & \frac{5}{36} & \frac{5}{36} - \frac{\sqrt{15}}{24} \\ \frac{1}{2} + \frac{\sqrt{15}}{10} & \frac{5}{36} + \frac{\sqrt{15}}{30} & \frac{2}{9} + \frac{\sqrt{15}}{15} \\ \hline & \frac{5}{18} & \frac{4}{9} \end{array}$	$\frac{5}{36}$
(C) IRK6	

TABLE 1. Butcher's Tableaus for the  $s$ -stage Gaussian-Legendre collocation Runge-Kutta methods with  $s = 1, 2, 3$ .

Denote  $I^m = I[u^m]$ ,  $M^m = M[u^m]$  and  $E^m = E[u^m, v^m]$  to be the invariant quantities from (2.3)-(2.5) at the time  $t = t_m$ . We have the following theorem.

**Theorem 3.1.** *The  $s$ -stage collocation Runge-Kutta method preserves the momentum (2.3), i.e.,*

$$I^{m+1} = I^m.$$

*Furthermore, the  $s$ -stage symplectic Runge-Kutta method (which is also called the quadratic preserving Runge-Kutta method) satisfies*

$$(3.3) \quad m_{ij} = b_i a_{ij} + b_j a_{ji} - b_i b_j = 0, \quad \text{for } i, j = 1, \dots, s,$$

*conserves the mass (2.4) and energy (2.5) exactly in the discrete time flow, i.e.,*

$$M^{m+1} = M^m, \quad \text{and} \quad E^{m+1} = E^m.$$

*Proof.* The proof is standard, similar to [18], [56] and [46]. Putting (3.2) in (2.3) yields

$$I^{m+1} - I^m = (u^{m+1} - u^m, 1) = \tau \left( \sum_{i=1}^s b_i f_i, 1 \right) = \tau \sum_{i=1}^s b_i (f_i, 1) = 0.$$

The last equality comes from the conservation law  $(f_i, 1) = (u_t, 1) = \frac{d}{dt}I = 0$  at each collocation time  $t = t_m + c_i\tau$  by the definition of the collocation Runge-Kutta method.

Similarly, putting (3.2) in (2.4), and using (3.1), yields

$$\begin{aligned} M^{m+1} &= (u^{m+1}, u^{m+1}) = (u^m + \tau \sum_{i=1}^s b_i f_i, u^m + \tau \sum_{i=1}^s b_i f_i) \\ &= (u^m, u^m) - 2\tau \sum_{i=1}^s b_i (f_i, \tau \sum_{j=1}^s a_{ij} f_j - U_j) + \tau^2 \sum_{i,j=1}^s b_i b_j (f_i, f_j) \\ &= M^m + 2\tau \sum_{i=1}^s b_i (f_i, U_i) - \tau^2 \sum_{i,j=1}^s (b_i a_{ij} + b_j a_{ji} - b_i b_j) (f_i, f_j) = M^m, \end{aligned}$$

since  $(f_i, U_i) = (u_t, u) = \frac{1}{2} \frac{d}{dt} M = 0$  at each collocation time  $t = t_m + c_i\tau$  from the conservation law in (2.4).

Similarly, to show  $E^{m+1} = E^m$ , we have

$$\begin{aligned} E^{m+1} &= -\frac{1}{2} (u_{xx}^{m+1}, u^{m+1}) - \frac{1}{p(p+1)} ((v^{m+1})^2 - C_0) \\ &= -\frac{1}{2} ((u^m + \tau \sum_{i=1}^s b_i f_i)_{xx}, u^m + \tau \sum_{i=1}^s b_i f_i) - \frac{1}{p(p+1)} ((v^m + \tau \sum_{i=1}^s b_i g_i)^2 - C_0) \\ &= -\frac{1}{2} (u_{xx}^m, u^m) - \frac{1}{p(p+1)} ((v^m)^2 - C_0) + \tau \sum_{i=1}^s b_i (\partial_x^2 f_i, U_i) + \tau \sum_{i=1}^s b_i \left( \frac{2}{p(p+1)} V_i g_i \right) \\ &\quad + \tau^2 \sum_{i,j=1}^s (b_i a_{ij} + b_j a_{ji} - b_i b_j) ((\partial_x^2 f_i, f_j) + g_i g_j) \\ &= E^m \end{aligned}$$

by  $(\partial_x^2 f_i, U_i) + \left( \frac{2}{p(p+1)} V_i g_i \right) = 0$  for each  $i$ , which follows from differentiating the conservation law (2.5) with respect to  $t$ . This completes the proof.  $\square$

From the theorem, we know that any arbitrary order of collocation Runge-Kutta method will conserve the momentum (2.3), the symplectic Runge-Kutta (SRK) method will conserve the mass (2.4) and energy (2.5) in the discrete time flow. Therefore, an arbitrarily high order time integrator can be constructed. In fact, from the proof of Theorem 3.1, reformulating the original equation (1.1) into the system (2.2) is only for the purpose of the energy conservation.

**3.2. A  $C_0$  adjustment process.** The key part for this SAV approach is to make sure that the term  $\int u^{p+1} dx + C_0$  is positive during the computational time  $t \in [0, T]$ . When considering the mKdV ( $p = 3$ ) case,  $\int u^{p+1} dx + C_0 > 0$  will automatically hold for any positive constant  $C_0$ , since  $p+1 = 4$  is even. This is also true for considering the nonlinear Schrödinger (NLS) equations or the Gross-Pitaevskii (GP) equations in [21] and [46], as the authors there only consider the cubic nonlinearity  $|u|^2 u$ , and thus,  $\int |u|^4 dx + C_0$  will automatically hold for any

constant  $C_0 > 0$ . However, when considering the KdV ( $p = 2$ ) case, a large enough constant  $C_0$  has to be set in the beginning of the simulation to guarantee  $v^2 := \int u^{p+1} dx + C_0 > 0$  for all  $t \in [0, T]$ . In the actual computation, it is not that simple to give a global estimation of  $\int u^{p+1} dx$  on  $t \in [0, T]$  prior to the simulation. However, we can adjust the value  $C_0$  at some time  $t = t_m$  if necessary.

Suppose at  $t = t_m$ ,  $\int (u^m)^{p+1} dx + C_0 < Tol$ , where  $Tol$  is a given positive number (e.g.,  $Tol = 5$ ). Then, we choose another constant  $\tilde{C}_0$  such that  $\int (u^m)^{p+1} dx + \tilde{C}_0 > Tol$ . For example, we can take  $\tilde{C}_0 = 10 - \int (u^m)^{p+1} dx$ , which leads to our new  $\tilde{v}^m \approx \sqrt{10}$ . Then, by using  $E[u^m, v^m] = E[u^m, \tilde{v}^m]$  from (2.5), we have our new  $\tilde{v}^m$

$$(3.4) \quad \tilde{v}^m = \sqrt{(v^m)^2 + \tilde{C}_0 - C_0}.$$

Finally, we substitute the  $v^m$  and  $C_0$  in (4.5) with  $\tilde{v}^m$  and  $\tilde{C}_0$ , and then, continue with the time evolution for  $t = t_{m+1}, t_{m+2}, \dots$ .

*Remark 3.1.* Note that  $v^2 = \int u^{p+1} dx + C_0$  holds only at the collocation points  $t = t_m + \tau c_i$  for each  $i = 1, 2, \dots, s$  in  $t \in [t_m, t_{m+1}]$ . However, the constant  $c_s$  may not necessarily equal to 0 or 1, e.g., see Table 1, which means  $v^2 = \int u^{p+1} dx + C_0$  does not hold at  $t_m$  in the discrete time flow. Therefore, the new  $\tilde{v}^m$  can only be evaluated by (3.4) to keep the discrete energy (2.5) invariant.

#### 4. SPATIAL DISCRETIZATION

In this section, we describe the spatial discretization. We show that the Fourier pseudo-spectral method will keep the momentum and energy invariant under such spatial discretization. Together with the temporal discretization in the previous section, the proposed scheme will preserve the discrete momentum and energy exactly in the discrete time flow. Moreover, we give an upper bound for the error of the discrete mass, which is caused by the spatial discretization.

Without loss of generality, we truncate the whole space into a bounded domain  $x \in [-L, L]$  for sufficiently large  $L$  with periodic boundary conditions at the boundary. We use the Fourier pseudo-spectral method to discretize the space because of the high-order accuracy and the application of the fast Fourier transform (FFT) (see. e.g., [61] and [65, Chapter 3]).

Now, we briefly introduce the spatial discretization strategy. Let  $N$  be the number of nodes and  $h = 2L/N$  to be the spatial step size. Denote  $x_j = hj$  and  $u_j \approx u(x_j)$  to be the spatial discretization for  $j = -N/2, \dots, N/2 - 1$ . By applying the standard discrete Fourier expansion, one obtains

$$(4.1) \quad u_j = \frac{1}{\sqrt{N}} \sum_{k=-N/2}^{N/2-1} \hat{u}_k e^{ik\pi x_j/L}, \quad \text{where} \quad \hat{u}_k = \frac{1}{\sqrt{N}} \sum_{j=-N/2}^{N/2-1} u_j e^{-ik\pi x_j/L}.$$

By introducing vectors  $\mathbf{u} = (u_{-N/2}, \dots, u_{N/2-1})^T$ ,  $\hat{\mathbf{u}} = (\hat{u}_{-N/2}, \dots, \hat{u}_{N/2-1})^T$ , and the discrete Fourier transform matrices

$$\mathbf{F}_{k,j} = \frac{1}{\sqrt{N}} e^{-ik\pi x_j/L}, \quad \mathbf{F}_{j,k}^{-1} = \frac{1}{\sqrt{N}} e^{ik\pi x_j/L}, \quad -N/2 \leq j, k \leq N/2 - 1.$$

One can write  $\mathbf{u}$  and  $\hat{\mathbf{u}}$  in a matrix form as  $\mathbf{u} = \mathbf{F}^{-1} \hat{\mathbf{u}}$  and  $\hat{\mathbf{u}} = \mathbf{F} \mathbf{u}$ . Also note that  $\mathbf{F}^{-1} = (\bar{\mathbf{F}})^T$ . Using the properties of the Fourier transform, one can easily obtain

$$u'_j = \frac{i\pi}{L} \sum_{k=-N/2}^{N/2-1} k \hat{u}_k e^{ik\pi x_j/L}, \quad u''_j = -\left(\frac{\pi}{L}\right)^2 \sum_{k=-N/2}^{N/2-1} k^2 \hat{u}_k e^{ik\pi x_j/L}.$$

Thus, we have the differential matrices  $\mathbf{D}_1$  and  $\mathbf{D}_2$ :

$$(4.2) \quad \mathbf{u}' = \mathbf{D}_1 \mathbf{u} = \bar{\mathbf{F}}^T \mathbf{\Lambda}_1 \mathbf{F} \mathbf{u}, \quad \text{and} \quad \mathbf{u}'' = \mathbf{D}_2 \mathbf{u} = \bar{\mathbf{F}}^T \mathbf{\Lambda}_2 \mathbf{F} \mathbf{u},$$

where  $\mathbf{\Lambda}_1 = i\mathbf{\Lambda}$ ,  $\mathbf{\Lambda}_2 = \mathbf{\Lambda}_1^2$ , and  $\mathbf{\Lambda} = \frac{\pi}{L} \text{diag}(-\frac{N}{2}, \dots, \frac{N-1}{2})$ . We note that  $\mathbf{D}_{1,2}$  are real matrices. Moreover, the matrix  $\mathbf{D}_2$  is symmetric. The matrix  $\mathbf{D}_1$  is antisymmetric ( $\mathbf{D}_1 = -\mathbf{D}_1^T$ ) and circulant, i.e.,  $\mathbf{D}_{1(j,k)} = d_{j-k}$ . Also note that both the row sum and the column sum of the matrix  $\mathbf{D}_1$  equal to 0, i.e., for each fixed  $k$  or  $j$ ,

$$(4.3) \quad \sum_{j=-N/2}^{N/2-1} d_{j,k} = \sum_{k=-N/2}^{N/2-1} d_{j,k} = 0.$$

This has been studied in many literatures, see e.g., [27] and [65, Chapter 3]. We remark here that in the actual computation,  $\mathbf{F}$  and  $\mathbf{F}^{-1}$  are not explicitly assembled, instead, the fast Fourier transform (FFT) is typically used in the computation.

For simplicity, if  $\mathbf{u}$  is a vector, we denote  $\mathbf{u}^p = (u_{-N/2}^p, u_{-N/2+1}^p, \dots, u_{N/2-1}^p)^T$  to be the pointwise power. Then, we define the discrete norms. Given two vectors  $\mathbf{u}, \mathbf{v}$ , define

$$(4.4) \quad (\mathbf{u}, \mathbf{v})_h = h \bar{\mathbf{v}}^T \mathbf{u} = h \sum_{j=-N/2}^{N/2-1} u_j \bar{v}_j, \quad \|\mathbf{u}\|_h = \sqrt{(\mathbf{u}, \mathbf{u})_h}.$$

Note that when  $\mathbf{u}, \mathbf{v} \in \mathbb{R}$ ,  $(\mathbf{u}, \mathbf{v})_h = (\mathbf{v}, \mathbf{u})_h$ . It is easy to see that  $(\mathbf{D}_2 \mathbf{u}, \mathbf{u})_h = (\mathbf{u}, \mathbf{D}_2 \mathbf{u})_h \in \mathbb{R}$ , since  $\mathbf{D}_2$  is real and symmetric. Also, we have  $(\mathbf{D}_1 \mathbf{u}, \mathbf{u})_h = (\mathbf{u}, \mathbf{D}_1 \mathbf{u})_h = 0$  from the antisymmetry of  $\mathbf{D}_1$ .

Denote  $v_h$  to be the spatial semi-discretization for  $v(t)$ , i.e.,  $v_h \approx v(t)$ . Then, the system of equations (2.2) is discretized into the following system

$$(4.5) \quad \begin{cases} \mathbf{u}_t = -\mathbf{D}_1 \left( \mathbf{D}_2 \mathbf{u} + \frac{1}{p} \frac{\mathbf{u}^p v_h}{\sqrt{(\mathbf{u}^p, \mathbf{u})_h + C_0}} \right) \equiv f(\mathbf{u}, v), \\ (v_h)_t = \frac{p+1}{2\sqrt{(\mathbf{u}^p, \mathbf{u})_h + C_0}} (\mathbf{u}^p, \mathbf{u}_t)_h \equiv g(\mathbf{u}, v). \end{cases}$$

Note that  $\mathbf{u}$  and  $f(\mathbf{u}, v_h)$  are an  $N \times 1$  vectors, and  $v_h$  and  $g(\mathbf{u}, v_h)$  are scalars.



Now, the spatial discrete momentum, mass and energy are defined as follows

$$(4.6) \quad I_h(\mathbf{u}) = (\mathbf{u}, \mathbf{1})_h;$$

$$(4.7) \quad M_h(\mathbf{u}) = (\mathbf{u}, \mathbf{u})_h;$$

$$(4.8) \quad E_h(\mathbf{u}, v_h) = -\frac{1}{2}(\mathbf{D}_2 \mathbf{u}, \mathbf{u})_h - \frac{1}{p(p+1)}(v_h^2 - C_0),$$

where  $\mathbf{1} = (1, 1, \dots, 1)^T$  is an  $N \times 1$  vector. We next obtain the conservation of the discrete momentum and energy, together with the error on the discrete mass.

**Theorem 4.1.** *The Fourier pseudo-spectral discretization to the equation (4.5) leads the following properties:*

$$(4.9) \quad \frac{d}{dt} I_h(\mathbf{u}) = 0; \quad \frac{d}{dt} E_h(\mathbf{u}, v_h) = 0.$$

Moreover,

$$(4.10) \quad \frac{d}{dt} M_h(\mathbf{u}) = -\frac{2h}{p} \mathbf{u}^T \mathbf{D}_1 \mathbf{u}^p.$$

*Proof.* Note that  $I_h \in \mathbb{R}$ , thus,

$$\frac{d}{dt} I_h(\mathbf{u}) = (\mathbf{u}_t, \mathbf{1})_h = (\mathbf{1}, \mathbf{u}_t).$$

We note that from (4.3), we have

$$\mathbf{1}^T \mathbf{D}_1 = \left( \sum_{k=-N/2}^{N/2-1} d_{-N/2,k}, \sum_{j=-N/2}^{N/2-1} d_{-N/2+1,k}, \dots, \sum_{j=-N/2}^{N/2-1} d_{N/2-1,k} \right) = \mathbf{0}^T.$$

Therefore, substitute  $\mathbf{u}_t$  by (4.5) yields

$$(4.11) \quad (\mathbf{u}_t, \mathbf{1})_h = h \mathbf{1}^T \mathbf{u}_t = -h \mathbf{1}^T \mathbf{D}_1 \left( \mathbf{D}_2 \mathbf{u} + \frac{1}{p} \frac{\mathbf{u}^p v_h}{\sqrt{(\mathbf{u}^p, \mathbf{u})_h + C_0}} \right) = 0.$$

Next, we prove  $\frac{d}{dt} E_h = 0$ , provided by  $v_h(v_h)_t = \frac{p+1}{2}(\mathbf{u}^p, \mathbf{u}_t)_h$  from (4.5), i.e.,

$$(4.12) \quad \begin{aligned} \frac{d}{dt} E_h &= -(\mathbf{D}_2 \mathbf{u}, \mathbf{u}_t)_h - \frac{2}{p(p+1)} v_h(v_h)_t = - \left( (\mathbf{D}_2 \mathbf{u}, \mathbf{u}_t)_h + \frac{1}{p} (\mathbf{u}^p, \mathbf{u}_t)_h \right) \\ &= \left( \mathbf{D}_2 \mathbf{u} + \frac{1}{p} \mathbf{u}^p, \mathbf{D}_1 (\mathbf{D}_2 \mathbf{u} + \frac{1}{p} \mathbf{u}^p) \right)_h = 0, \end{aligned}$$

since  $\mathbf{D}_1$  is antisymmetric.

For proving (4.10), we first note that  $\mathbf{D}_1 \mathbf{D}_2 = \mathbf{D}_2 \mathbf{D}_1$  from the decomposition in (4.2). Then,  $(\mathbf{D}_1 \mathbf{D}_2 \mathbf{u}, \mathbf{u})_h = -(\mathbf{D}_2 \mathbf{u}, \mathbf{D}_1 \mathbf{u})_h$  from the antisymmetry of  $\mathbf{D}_1$ . On the other hand,

$(\mathbf{D}_1 \mathbf{D}_2 \mathbf{u}, \mathbf{u})_h = (\mathbf{D}_2 \mathbf{D}_1 \mathbf{u}, \mathbf{u})_h = (\mathbf{D}_2 \mathbf{u}, \mathbf{D}_1 \mathbf{u})_h$ . Therefore,  $(\mathbf{D}_1 \mathbf{D}_2 \mathbf{u}, \mathbf{u})_h = 0$ . Also, note that  $\frac{v_h}{\sqrt{(\mathbf{u}^p, \mathbf{u})_h + C_0}} = 1$  in the continuous time. Then,

$$(4.13) \quad \begin{aligned} \frac{d}{dt} M_h &= 2(\mathbf{u}_t, \mathbf{u})_h = -2(\mathbf{D}_1 \mathbf{D}_2 \mathbf{u}, \mathbf{u})_h - \frac{2}{p}(\mathbf{D}_1 \mathbf{u}^p, \mathbf{u})_h \\ &= -\frac{2}{p}(\mathbf{D}_1 \mathbf{u}^p, \mathbf{u})_h = -\frac{2h}{p} \mathbf{u}^T \mathbf{D}_1 \mathbf{u}^p, \end{aligned}$$

which completes the proof.  $\square$

Theorem 4.1 shows that in the continuous time flow, the spatial discretization will keep the momentum (2.3) and energy (2.5) invariant in their corresponding discrete sense. However, the time derivative on the discrete mass (4.10) is not necessarily 0. We next show that the proposed scheme conserves the discrete momentum and energy, and also give an error estimate of the discrete mass.

From Theorem 4.1, we have the following little corollary.

**Corollary 4.1.** *Suppose  $(\mathbf{u}, v_h)$  is the solution to (4.5), then we have*

$$(4.14) \quad (f(\mathbf{u}, v_h), \mathbf{1})_h = 0,$$

$$(4.15) \quad -(\mathbf{D}_2 \mathbf{u}, f(\mathbf{u}, v_h))_h - \frac{2}{p(p+1)} v_h g(\mathbf{u}, v_h) = 0,$$

$$(4.16) \quad (f(\mathbf{u}, v_h), \mathbf{u})_h = -\frac{2h}{p} \mathbf{u}^T \mathbf{D}_1 \mathbf{u}^p.$$

*Proof.* Substituting  $\mathbf{u}_t = f(\mathbf{u}, v_h)$  in the equation (4.11) and (4.13) yields (4.14) and (4.16), respectively. From (4.12), we have

$$0 = \frac{d}{dt} E_h = -(\mathbf{D}_2 \mathbf{u}, \mathbf{u}_t)_h - \frac{2}{p(p+1)} v_h (v_h)_t = -(\mathbf{D}_2 \mathbf{u}, f(\mathbf{u}, v_h))_h - \frac{2}{p(p+1)} v_h g(\mathbf{u}, v_h),$$

which completes the proof.  $\square$

Define the full discretization in space and time  $u_j^m \approx u(x_j, t_m)$  and  $v_h^m \approx v(t_m)$ . Then, denote  $\mathbf{u}^m$  and  $v_h^m$  to be the numerical solution to (4.5). Define the discrete momentum, mass and energy as follows:

$$(4.17) \quad I_h^m = (\mathbf{u}^m, \mathbf{1})_h;$$

$$(4.18) \quad M_h^m = (\mathbf{u}^m, \mathbf{u}^m)_h;$$

$$(4.19) \quad E_h^m = -\frac{1}{2}(\mathbf{D}_2 \mathbf{u}^m, \mathbf{u}^m)_h - \frac{1}{p(p+1)} ((v_h^m)^2 - C_0).$$

The following theorem shows the conservation of the discrete momentum (4.17) and the discrete energy (4.19) for the proposed scheme. It also shows the upper bound of the error for the discrete mass (4.18).

**Theorem 4.2.** *Suppose the discretized system (4.5) is solved by the  $s$ -stage symplectic Runge-Kutta method which satisfies (3.3), then the solution  $\mathbf{u}^m$  and  $v_h^m$  to the equation (4.5) satisfies*

$$(4.20) \quad I_h^{m+1} = I_h^m; \quad E_h^{m+1} = E_h^m.$$

*In the meanwhile, denote  $U_i^m$  and  $V_i^m$  to be the intermediate step for the SRK method at  $t = t_m + c_i\tau$ . Also note that  $U_i^m \approx \mathbf{u}^m$ , then*

$$(4.21) \quad |M_h^m - M_h^0| \leq t_m \frac{4h}{p} \max_{1 \leq \nu \leq m, 1 \leq i \leq s} |(U_i^\nu)^\mathbf{T} \mathbf{D}_1 (U_i^\nu)^\mathbf{P}| \approx t_m \frac{4h}{p} \max_{1 \leq \nu \leq m} |(\mathbf{u}^\mathbf{T})^\nu \mathbf{D}_1 (\mathbf{u}^\mathbf{P})^\nu|.$$

*Proof.* The conservation (4.20) are obtained from substituting the continuous variables and inner products in Theorem 3.1 with the spatial discrete sense (4.4), and substitute  $\mathbf{u}$  in the equations (4.14) and (4.15) in Collary 4.1 by  $U_i^m$  and  $V_i^m$ , since they are intermediate steps which satisfy the equation (4.5) exactly.

For (4.21), by substituting the continuous variables and inner products into the spatial discrete sense and use (4.16) yields

$$\begin{aligned} M_h^m - M_h^{m-1} &= 2\tau \sum_{i=1}^s b_i (f_i, U_i^{m-1})_h = -2\tau \sum_{i=1}^s b_i \frac{2h}{p} (U_i^{m-1})^\mathbf{T} \mathbf{D}_1 (U_i^{m-1})^\mathbf{P} \\ &\leq \frac{4\tau h}{p} \max_{1 \leq i \leq s} |(U_i^{m-1})^\mathbf{T} \mathbf{D}_1 (U_i^{m-1})|, \end{aligned}$$

since  $\sum_{i=1}^s b_i = 1$ . Therefore,

$$\begin{aligned} |M_h^m - M_h^0| &= \left| \sum_{\nu=1}^m (M_h^\nu - M_h^{\nu-1}) \right| \leq \sum_{\nu=1}^m |M_h^\nu - M_h^{\nu-1}| \leq \frac{4\tau h}{p} \sum_{\nu=1}^m \max_{1 \leq i \leq s} |(U_i^\nu)^\mathbf{T} \mathbf{D}_1 (U_i^\nu)| \\ &\leq \frac{4\tau h}{p} \sum_{\nu=1}^m \max_{1 \leq \nu \leq m, 1 \leq i \leq s} |(U_i^\nu)^\mathbf{T} \mathbf{D}_1 (U_i^\nu)| = \frac{4t_m h}{p} \max_{1 \leq \nu \leq m, 1 \leq i \leq s} |(U_i^\nu)^\mathbf{T} \mathbf{D}_1 (U_i^\nu)|, \end{aligned}$$

the last equality comes from  $t_m = m\tau$  and completes the prove.  $\square$

Theorem 4.2 shows that the discrete momentum and energy will be preserved exactly for the proposed scheme. In the meanwhile, the inequality (4.21) shows the upper bound for the error of the discrete mass, which grows linearly with respect to time. However, note that the term  $h\mathbf{u}^\mathbf{T} \mathbf{D}_1 \mathbf{u}^\mathbf{P}$  is the Fourier spectral approximation of the integral  $\frac{1}{p+1} \int (u^{p+1})_x dx$ , i.e.,

$$h\mathbf{u}^\mathbf{T} \mathbf{D}_1 \mathbf{u}^\mathbf{P} \approx ((u^p)_x, u) = \frac{1}{p+1} ((u^{p+1})_x, 1) = 0.$$

Therefore, instead of decreasing in the 1st order with respect to  $h$ , the term  $|h\mathbf{u}^\mathbf{T} \mathbf{D}_1 \mathbf{u}^\mathbf{P}|$  is of spectral accuracy and very small (generally on the order of  $10^{-14}$ ), which is usually several order lower than the tolerance of the fixed point solver for the resulting nonlinear system. As a consequence, the error of the discrete mass becomes unnoticeable during our simulation even up to the time  $t_m = 200$ , see details in the next section.

## 5. NUMERICAL EXAMPLES

**5.1. A fast solver.** In this section, we show numerical examples for the proposed scheme. Before illustrating the examples, we describe a fast solver for solving the resulting nonlinear system from the IRK methods. This fast solver is similar to the one in [21], which is based on the fixed point iteration. It is on the same order of the computational cost in solving the original equation, despite of the new auxiliary variable being introduced. To be specific, we consider the IRK4 ( $s = 2$ ) case. The other cases can be easily generalized. We introduce the auxillary variables and rewrite the system as

$$(5.1) \quad \begin{cases} U_i = \mathbf{u}^m + \tau \sum_{j=1}^2 a_{ij} \mathbf{f}_j, \\ \Phi_i = \frac{(U_i)^p}{\sqrt{((U_i)^p, U_i)_h + C_0}}, \quad g_i = \frac{p+1}{2} (\Phi_i, \mathbf{f}_i)_h, \\ V_i = v_h^m + \tau \sum_{j=1}^2 a_{ij} g_j, \quad i = 1, 2, \end{cases}$$

and

$$(5.2) \quad \begin{cases} \mathbf{f}_1 = -\mathbf{D}_1 \left( \mathbf{D}_2(\mathbf{u}^m + \tau \sum_{j=1}^2 a_{1j} \mathbf{f}_j) + \frac{1}{p} \Phi_1 V_1 \right), \\ \mathbf{f}_2 = -\mathbf{D}_1 \left( \mathbf{D}_2(\mathbf{u}^m + \tau \sum_{j=1}^2 a_{2j} \mathbf{f}_j) + \frac{1}{p} \Phi_2 V_2 \right). \end{cases}$$

Then,  $\mathbf{u}^{m+1}$  and  $v_h^{m+1}$  can be updated by (3.2).

The system (5.1) and (5.2) can be solved by the fixed point iteration. At the  $l$ th iteration, we have

$$(5.3) \quad \begin{cases} (\mathbf{I} + \tau a_{11} \mathbf{D}_3) \mathbf{f}_1^{l+1} + \tau a_{12} \mathbf{D}_3 \mathbf{f}_2^{l+1} = -(\mathbf{D}_3 \mathbf{u}^m - \frac{1}{p} \mathbf{D}_1 (\Phi_1^l V_1^l)), \\ \tau a_{21} \mathbf{D}_3 \mathbf{f}_1^{l+1} + (\mathbf{I} + \tau a_{22} \mathbf{D}_3) \mathbf{f}_2^{l+1} = -(\mathbf{D}_3 \mathbf{u}^m - \frac{1}{p} \mathbf{D}_1 (\Phi_2^l V_2^l)), \end{cases}$$

where  $\mathbf{I}$  is the identity matrix and  $\mathbf{D}_3 = \mathbf{D}_1 \mathbf{D}_2$ . The system (5.3) can be first transformed into the sparse matrix by FFT, and then we apply the standard sparse matrix solvers. The leading order of the computational cost is  $\mathcal{O}(N \log(N))$  from the FFT for the matrices  $\mathbf{D}_{1,3}$ . After obtaining  $\mathbf{f}_i^{l+1}$ , we can use (5.1) to obtain the values of other variables  $U_i^{l+1}$ ,  $\Phi_i^{l+1}$ ,  $g_i^{l+1}$ , and  $V_i^{l+1}$ . The total computational cost remains on the same order.

We set  $\mathbf{f}_1^0 = \mathbf{f}_2^0 = f(\mathbf{u}^m, v_h^m)$  to start the iteration, and the iteration terminates when

$$\max_i \|\mathbf{f}_i^{l+1} - \mathbf{f}_i^l\|_\infty < \epsilon,$$

where  $i = 1, 2$ , and  $\epsilon$  is typically set to be  $10^{-12}$  in our simulations.

In general, for the  $s$ -stage Runge-Kutta method, the computational cost is always on the order of  $\mathcal{O}(s \times N \log(N))$ . The  $s$ -stage Gaussian-Legendre collocation methods will obtain the order of  $2s$  on temporal accuracy, which is the maximum for the RK methods. Thus, we only use the  $s$ -stage Gaussian-Legendre collocation methods as in Table 1 in our examples.

**5.2. Numerical examples.** In this section, we list our numerical examples by using the proposed scheme. The  $s$ -stage implicit Gaussian-Legendre Runge-Kutta methods as in Table 3.1 are typically used, which are denoted by IRK2-SAV, IRK4-SAV and IRK6-SAV,

respectively. For a comparison, the equation (1.1) is also solved directly by the 4th order Exponential Time Differencing (mETDRK4) method from [37], which is non-conservative; note that the IRK2, IRK4 and IRK6 methods conserve the momentum and mass in the discrete time. We track the following quantities at  $t = t_m$  to check the accuracy by

$$(5.4) \quad \mathcal{E}^m = \|u_{exact}^m - \mathbf{u}^m\|_\infty;$$

$$(5.5) \quad \mathcal{E}_I^m = |I_h^m - I_h^0|;$$

$$(5.6) \quad \mathcal{E}_M^m = \max_{j < m} |M_h^j - M_h^0|;$$

$$(5.7) \quad \mathcal{E}_E^m = \max_{j < m} |E_h^j - E_h^0|.$$

*Remark 5.1.* Defining the error in the form (5.5) will be too oscillatory. Therefore, to have a clearer picture, we define the error of the discrete mass and energy as in (5.6) and (5.7), which makes the errors non-decreasing over time.

*Example 1.* Our first example is to consider the KdV ( $p = 2$ ) equation with two solitons. The exact solution satisfies

$$(5.8) \quad u(x, t) = 12 \frac{\gamma_1^2 e^{\theta_1} + \gamma_2^2 e^{\theta_2} + 2(\gamma_2 - \gamma_1)^2 e^{\theta_1 + \theta_2} + a^2(\gamma_2^2 e^{\theta_1} + \gamma_1^2 e^{\theta_2}) e^{\theta_1 + \theta_2}}{(1 + e^{\theta_1} + e^{\theta_2} + a^2 e^{\theta_1 + \theta_2})^2},$$

where we take the parameters

$$\begin{aligned} \gamma_1 &= 0.4, \quad \gamma_2 = 0.6, \quad a^2 = \left( \frac{\gamma_1 - \gamma_2}{\gamma_1 + \gamma_2} \right)^2 = \frac{1}{25}, \\ \theta_1 &= \gamma_1 x - \gamma_1^3 t + x_1, \quad \theta_2 = \gamma_2 x - \gamma_2^3 t + x_2, \quad x_1 = 10, \quad x_2 = 25. \end{aligned}$$

This initial condition represents two solitons, a larger one is on the left of the smaller one (see the left subplot in Figure 1). Both of the solitons travel to the right. The larger soliton travels with faster speed, and thus, will catch up with the smaller one. Then, they are supposed to merge and split again. The example is from [70]. We take  $L = 30\pi$  with  $N = 2048$  in space. The time step is taken to be  $\tau = 0.1$  and the stopping time  $T = 200$ . Figure 1 shows the solution profile obtained by the IRK4-SAV method. The left subplot is the initial condition  $u_0$ , the right subplot is the time evolution. One can see that the solitons travel to the right with different speeds, intersect, and then split again with their initial speeds. This is similar to the result in [70].

Figure 2 tracks the results obtained by different time integrators. The top left subplot in Figure 2 shows  $\|\mathbf{u}^m - u_{exact}\|_\infty$  with respect to time, where  $u_{exact} = u(\mathbf{x}, t_m)$  is the exact solution. One can see that the error by using the mETDRK4 method is between the error by IRK2 type methods (IRK2 and IRK2-SAV) and IRK4 type methods (IRK4 and IRK4-SAV). This is resonable, since IRK2 methods are of the second order accuracy in time, whereas the rest three are of the 4th order accuracy in time. The two IRK2 methods (IRK2 and

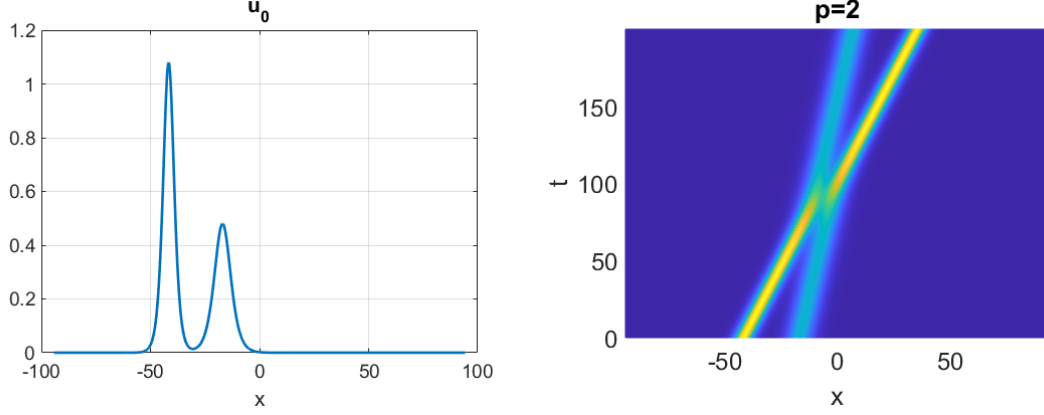


FIGURE 1. The solution profile for Example 1 from IRK4-SAV. Left:  $u_0$ . Right:  $u(x, t)$  from the top view.

IRK2-SAV) and IRK4 methods (IRK4 and IRK4-SAV) are indistinguishable from each other in the subplot. The zoomed picture in Figure 3 shows the tiny differences.

The top right subplot in Figure 2 tracks the error of the discrete momentum (5.5) at different times. One can see that it stays around the level  $10^{-13}$  for all time integrators that we apply here. The error is as expected for the IRK2 and IRK4 types of methods, since they have been proved to conserve this quantity in Theorem 3.1. Moreover, the mETDRK4 method also preserves the discrete momentum according to the numerical result.

The bottom two subplots in Figure 2 track the error of discrete mass (5.6) and energy (5.7), respectively. One can see that except for the mETDRK4, the other four schemes keep the error of the discrete mass  $\mathcal{E}_M^m$  around or below the level of  $10^{-12}$ . Note that the tolerance for solving the resulting nonlinear system (5.3) is set to be  $10^{-12}$ . Thus, the error level justifies that the schemes conserve the quantities as theoretically proved in Theorem 3.1. This also shows that the error of discrete mass in Theorem 4.2 is very small, even smaller than our fixed point solver tolerance ( $10^{-12}$ ), since such error is unnoticeable from the numerical results.

The bottom right subplots tracks the error of the discrete energy. One can see that the IRK2 method has the largest error, since the IRK2 method has the lowest order of temporal accuracy. On the other hand, once we switch to the IRK2-SAV approach, despite of an almost the same  $L^\infty$  error as for the IRK2 method, the discrete energy error drops to the level  $10^{-13}$ , and becomes competitive with the IRK4-SAV method. This shows that the error comes from solving the nonlinear system (5.3), and agrees with the result in Theorem 4.2.

We also list the  $L^\infty$  error  $\mathcal{E}^m$  for the IRK2-SAV and IRK4-SAV methods from different time steps  $\tau$  in Table 2. One can see that the error for IRK2-SAV method decreases at the second order speed, and the error for IRK4-SAV method decreases at the 4th order speed, except for  $\tau = \frac{1}{40}$ , where the temporal error is too close to the error of solving the nonlinear

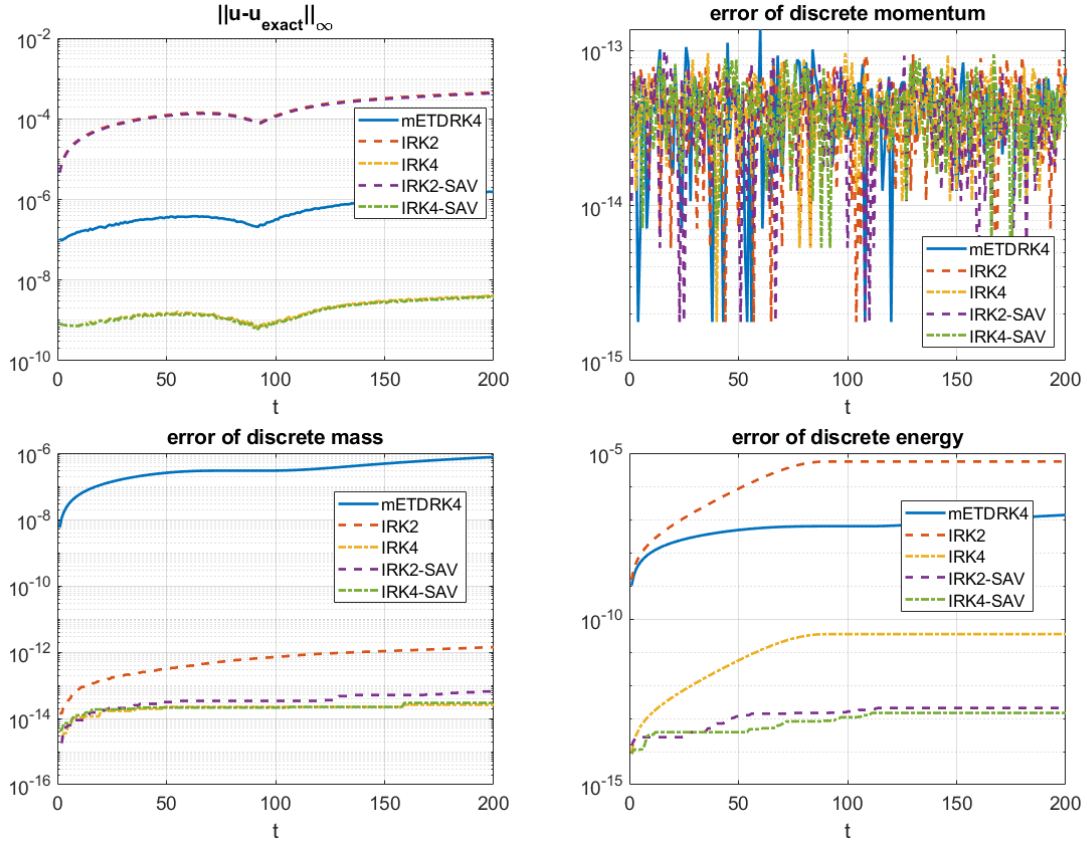


FIGURE 2. The errors in Example 1 by different time integrators: mETDRK (solid blue); IRK2(dash red); IRK2-SAV (dash purple); IRK4 (dash dot orange); IRK4-SAV (dash dot green). Top left:  $\|u - u_{\text{exact}}\|_{\infty}$ . Top right: discrete momentum error. Bottom left: discrete mass error. Bottom right: discrete energy error.

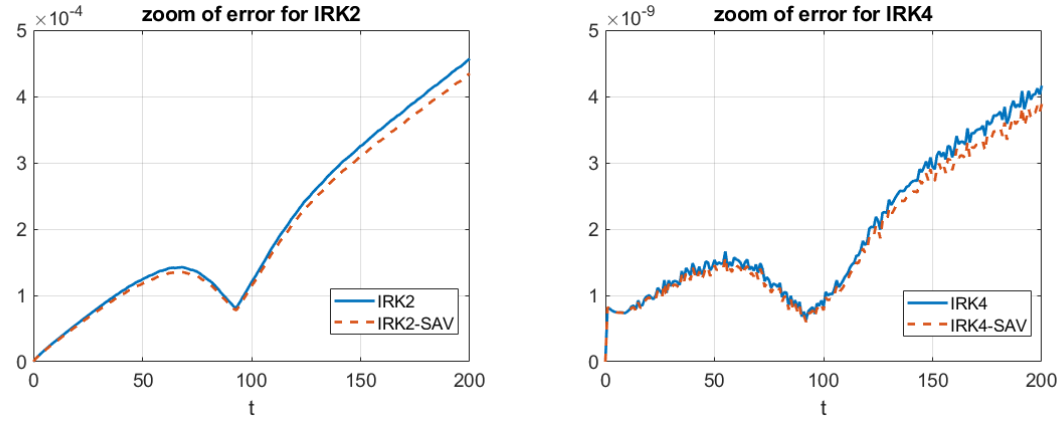


FIGURE 3. Zoom-in into the errors presented in Figure 2 for IRK2 and IRK4.

	IRK2-SAV		IRK4-SAV	
$\tau$	error	rate	error	rate
$\frac{1}{5}$	$1.7e-3$	NA	$6.40e-8$	NA
$\frac{1}{10}$	$4.3e-4$	3.998	$3.89e-9$	16.47
$\frac{1}{20}$	$1.1e-4$	3.998	$2.47e-10$	15.75
$\frac{1}{40}$	$2.72e-5$	4.001	$1.78e-11$	13.82

TABLE 2. The convergence rates of IRK2-SAV and IRK4-SAV in Example 1.

system, and thus, affects the final results. Therefore, the IRK2-SAV and IRK4-SAV are still of the 2nd order and the 4th order temporal accuracy, respectively.

*Example 2.* We next consider the scattering solution for the KdV equation with the initial condition  $u_0 = -\text{sech}^2(x)$ . This example is a soliton type data with negative sign, which has been studied, for example, in [40]. The KdV evolution will lead  $u_0$  to the dispersion, and possible negative value for  $\int u^3 dx$ . Here, the  $C_0$  adjustment process in (3.4) will make  $v(t)$  stay positive, and thus, will keep the algorithm applicable for all times. The exact solution is not explicitly given, since it is not exactly the soliton due to the negative sign and coefficients chosen. We compute the reference solution  $u_{ref}$  by both mETDRK4 and IRK4-SAV methods separately with an ultimately small time step ( $\tau = 1/25600$ ). The results from these two different approaches differ at the level of  $10^{-12}$ . Therefore, we can take the reference solution as the “exact” solution. In the simulation, we take  $\tau = 0.01$ , with  $L = 30\pi$  and  $N = 2048$ , the same as in the previous example.

The left subplot in Figure 4 shows the solution profile evolving in time. One can see that it disperses to the left. The right subplot shows the solution profile at the stopping time  $T = 1$ . The fast oscillations on the left can be observed. Figure 5 tracks the data in (5.4)-(5.7) that we are interested in.

The top right subplot in Figure 5 shows that the momentum is conserved for all these five approaches. The bottom subplots tracks the errors of mass and energy. The results are as expected and similar to the Example 1.

Table 3 shows the convergence rates for all these five time integrators. From Table 3, we find that the convergence rates is lower than the expected rate for all these approaches. However, as the time step  $\tau$  decreases, the rates are approaching their theoretical values (4 for the 2nd order methods and 16 for the 4th order methods). The sub-convergence rate is most likely caused by the fast oscillations of the solution as well as insufficiently small  $\tau$ .

*Example 3.* Our final example considers the mKdV ( $p = 3$ ) and gKdV ( $p = 4$ ) equations. These cases admit a family of soliton solutions  $u(x, t) = Q_c(x - ct - x_0)$  traveling with a constant speed  $c$ , and  $Q_c = \left( \frac{cp(p+1)}{2} \text{sech}^2\left(\frac{\sqrt{c}(p-1)}{2}x\right) \right)^{\frac{1}{p-1}}$  being the soliton solution from the



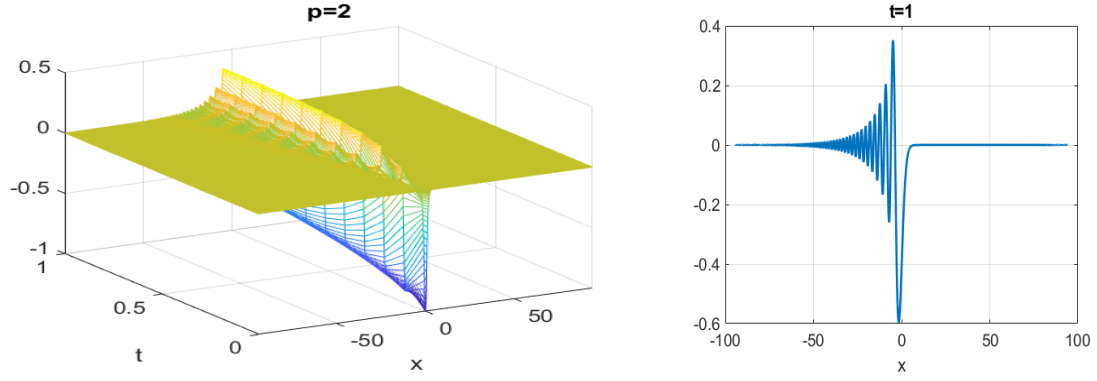


FIGURE 4. The solution profile in Example 2 from IRK4-SAV. Left:  $u(x, t)$ . Right:  $u(x, t)$  at  $t = 1$ .

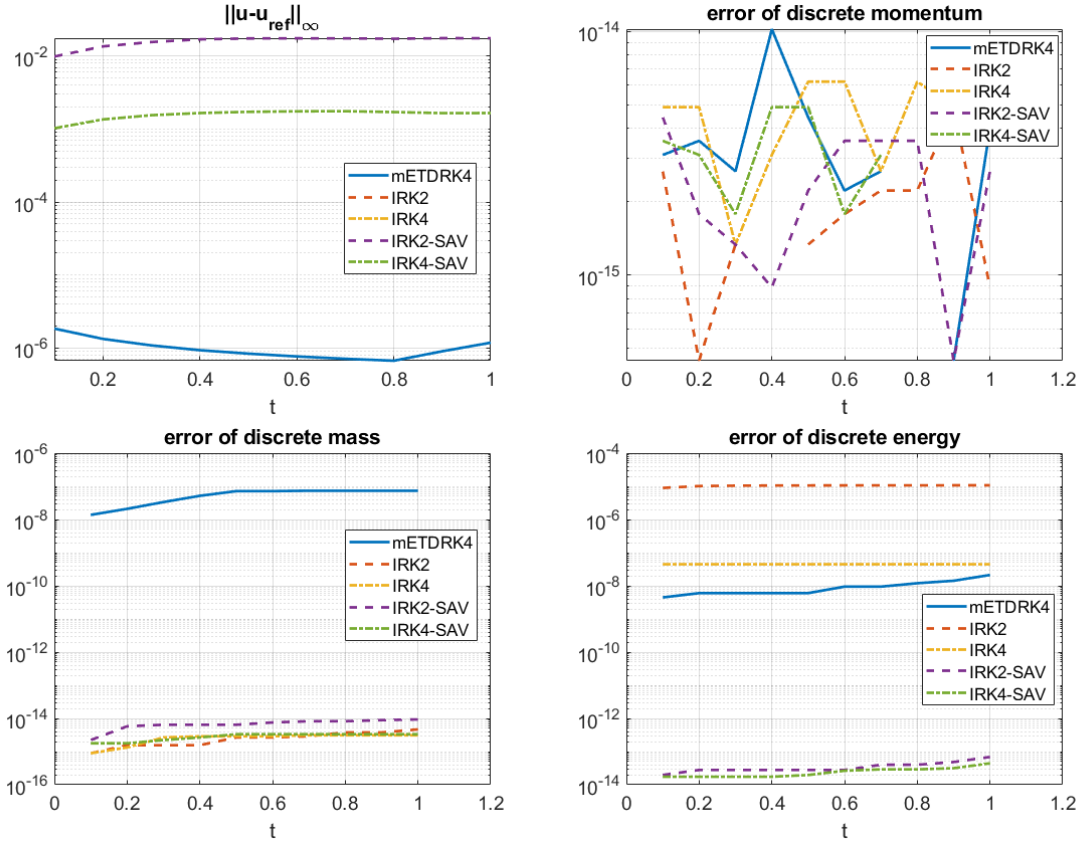


FIGURE 5. The errors for Example 2 by different time integrators: mET-DEK4 (solid blue); IRK2(dash red); IRK2-SAV (dash purple); IRK4 (dash dot orange); IRK4-SAV (dash dot green). Top left:  $\|u - u_{ref}\|_{\infty}$ . Top right: discrete momentum error. Bottom left: discrete mass error. Bottom right: discrete energy error.

	mETDRK4		IRK2		IRK4		IRK2-SAV		IRK4-SAV	
$\tau$	error	rate	error	rate	error	rate	error	rate	error	rate
$\frac{1}{100}$	$1.85e-6$	NA	$1.76e-2$	NA	$1.76e-3$	NA	$1.76e-2$	NA	$1.76e-3$	NA
$\frac{1}{200}$	$1.34e-7$	13.81	$6.38e-3$	2.76	$2.85e-4$	6.18	$6.38e-3$	2.76	$2.85e-4$	6.18
$\frac{1}{400}$	$1.12e-8$	11.96	$2.09e-3$	3.04	$3.74e-5$	7.63	$2.09e-3$	3.04	$3.74e-5$	7.63
$\frac{1}{800}$	$7.74e-10$	14.45	$6.01e-4$	3.49	$3.63e-6$	10.28	$6.01e-4$	3.49	$3.63e-6$	10.28

TABLE 3. The convergence rates of mETDRK, IRK2, IRK4, IRK2-SAV and IRK4-SAV in Example 2. We can see the errors are the same in the IRK2 types of methods and IRK4 types of methods up to the second decimal.

equation

$$-Q_{xx} + cQ - \frac{1}{p}Q^p = 0.$$

We refer to [51], [41] for more details. We take  $c = 1$ ,  $x_0 = -50$  and  $\tau = 0.05$ . The equation is solved by mETDRK4, IRK2-SAV, IRK4-SAV and IRK6-SAV methods. The simulation ends at  $T = 100$ .

Figure 6 shows the solution profiles for  $p = 3$  (left) and  $p = 4$  (right) obtained from IRK4-SAV method. The solution travels in the soliton manner as expected. While the mETDRK4 method fails to capture the soliton behavior for both  $p = 3$  and  $p = 4$  at the current time step size ( $\tau = 0.05$ ), the other three conservative methods capture such phenomenon quite well, see Figure 7. Figures 8 and 9 track the  $L^\infty$ -errors  $\mathcal{E}^m$ ,  $\mathcal{E}_I^m$ ,  $\mathcal{E}_M^m$  and  $\mathcal{E}_E^m$  for  $p = 3$  and  $p = 4$ , respectively. The top-left subplot shows that the mETDRK has the poorest performance, since it fails to capture the soliton behavior. The IRK6-SAV method is the most accurate among them as expected. The top-right subplot shows that the discrete momentum is conserved for all these four approaches, which is consistent with the KdV cases in Examples 1 and 2. The bottom two subplots track the error of discrete mass and energy. All these quantities preserve well as expected, showing the effectiveness of our proposed algorithm.

## 6. CONCLUSION

We propose a numerical algorithm for the generalized KdV equations, which can preserve all the three invariant quantities in the discrete time flow with an arbitrarily high order of temporal accuracy. This is based on the scalar auxillary variable (SAV) approach. By reformulating a considered equation, the energy can be rewritten into the sum of two quadratic terms. Therefore, any quadratic preserving (symplectic) Runge-Kutta method can preserve all the three invariant quantities in the discrete time evolution. With the Fourier pseudo-spectral discretization in space, the discrete momentum and energy can be preserved exactly. While the Fourier pseudo-spectral discretization causes the error in discrete mass, it remains very small, generally on the lower order of the fixed point solver tolerance, and thus, becomes unnoticeable in our numerical experiments. Our numerical simulations show the high accuracy and efficiency of the proposed scheme.

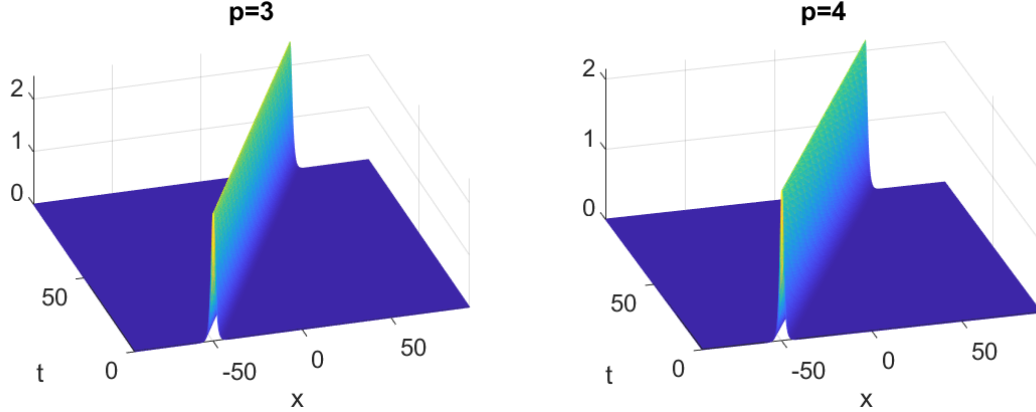


FIGURE 6. The solution profile in Example 3 from IRK4-SAV. Left:  $p = 3$ . Right:  $p = 4$ .

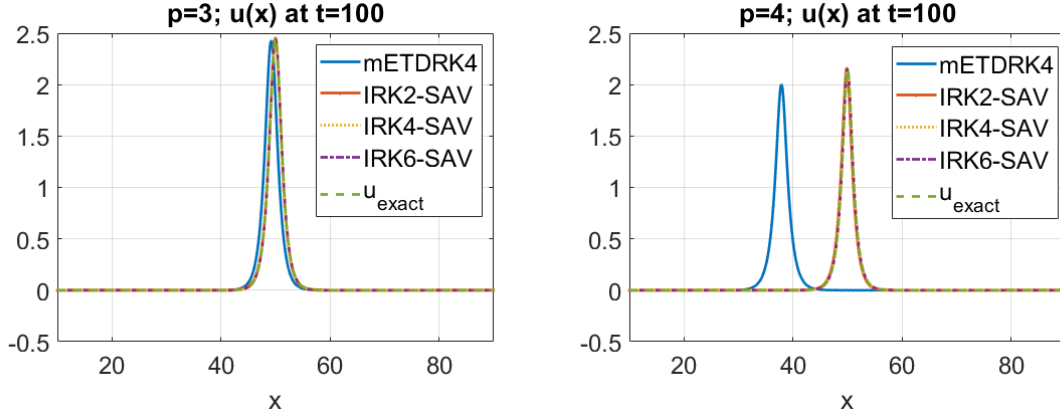


FIGURE 7. Example 3: solution at  $t = 100$  from different time integrators mETDEK4 (solid blue); IRK2-SAV (dot solid red); IRK4-SAV (dot orange); IRK6-SAV (dot dash purple); exact solution (dash green). Left:  $p = 3$ . Right:  $p = 4$ .

## REFERENCES

- [1] L. Abdelouhab, J. Bona, M. Felland, and J.-C. Saut. Nonlocal models for nonlinear, dispersive waves. *Physica D: Nonlinear Phenomena*, 40(3):360–392, 1989.
- [2] A. Alazman, J. Albert, J. Bona, M. Chen, J. Wu, et al. Comparisons between the BBM equation and a Boussinesq system. *Advances in Differential Equations*, 11(2):121–166, 2006.
- [3] M. Alexander and J. L. Morris. Galerkin methods applied to some model equations for non-linear dispersive waves. *Journal of Computational Physics*, 30(3):428–451, 1979.
- [4] D. N. Arnold and R. Winther. A superconvergent finite element method for the Korteweg-de-Vries equation. *Mathematics of Computation*, 38(157):23–36, 1982.
- [5] G. A. Baker, V. A. Dougalis, and O. A. Karakashian. Convergence of Galerkin approximations for the Korteweg-de-Vries equation. *Mathematics of Computation*, 40(162):419–433, 1983.

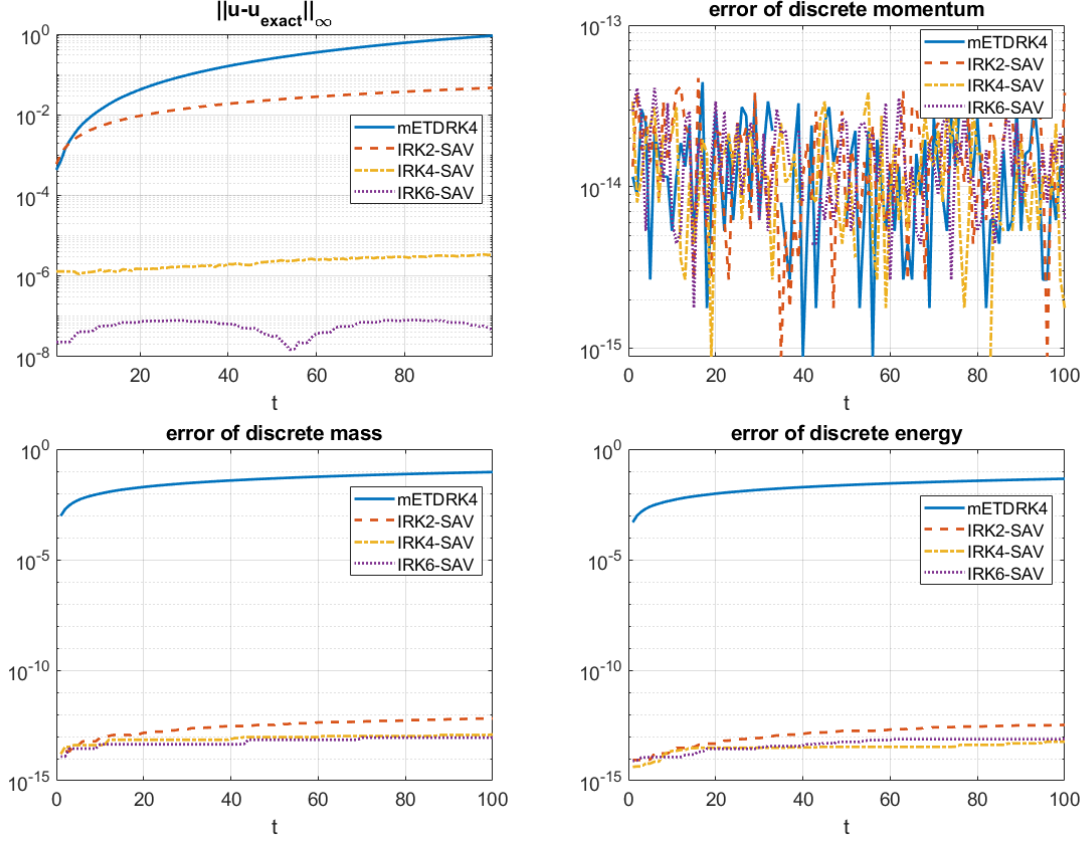


FIGURE 8. The errors in Example 3 with  $p = 3$  by different time integrators: mETDEK4 (solid blue); IRK2(dash red); IRK2-SAV (dash purple); IRK4 (dash dot orange); IRK4-SAV (dash dot green). Top left:  $\|u - u_{exact}\|_{\infty}$ . Top right: discrete momentum error. Bottom left: discrete mass error. Bottom right: discrete energy error.

- [6] T. B. Benjamin, J. L. Bona, and J. J. Mahony. Model equations for long waves in nonlinear dispersive systems. *Philosophical Transactions of the Royal Society of London. Series A, Mathematical and Physical Sciences*, 272(1220):47–78, 1972.
- [7] J. Bona, H. Chen, O. Karakashian, and Y. Xing. Conservative, discontinuous Galerkin–methods for the generalized Korteweg-de Vries equation. *Mathematics of Computation*, 82(283):1401–1432, 2013.
- [8] J. Bona, V. Dougalis, O. Karakashian, W. McKinney, and F. Smith. Conservative, high-order numerical schemes for the generalized Korteweg-de-Vries equation. *Philosophical Transactions of the Royal Society of London. Series A: Physical and Engineering Sciences*, 351(1695):107–164, 1995.
- [9] J. Bona, W. Pritchard, and L. Scott. An evaluation of a model equation for water waves. *Philosophical Transactions of the Royal Society of London. Series A, Mathematical and Physical Sciences*, 302(1471):457–510, 1981.
- [10] J. L. Bona. On solitary waves and their role in the evolution of long waves. *Applications of nonlinear analysis in the physical sciences*, pages 183–205, 1981.

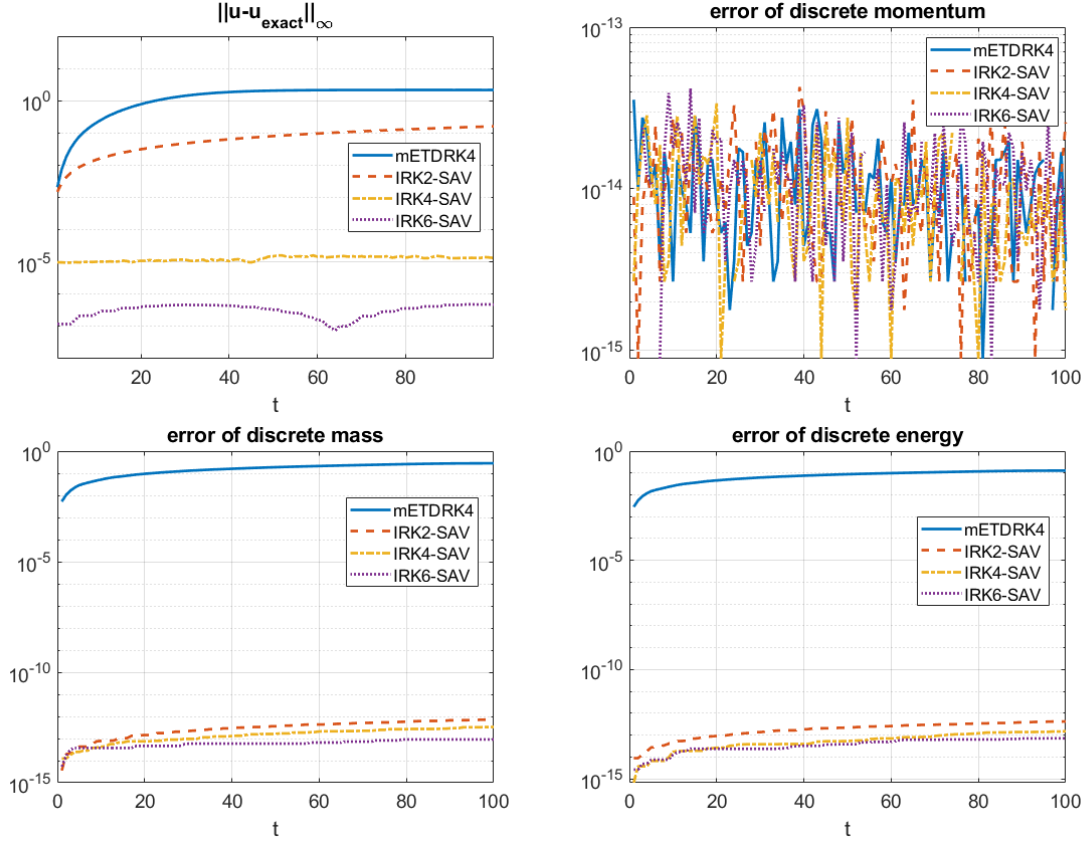


FIGURE 9. The errors for Example 3 with  $p = 4$  by different time integrators: mETDEK4 (solid blue); IRK2(dash red); IRK2-SAV (dash purple); IRK4 (dash dot orange); IRK4-SAV (dash dot green). Top left:  $\|u - u_{\text{exact}}\|_{\infty}$ . Top right: discrete momentum error. Bottom left: discrete mass error. Bottom right: discrete energy error.

- [11] J. L. Bona, T. Colin, and D. Lannes. Long wave approximations for water waves. *Archive for rational mechanics and analysis*, 178(3):373–410, 2005.
- [12] J. L. Bona, V. A. Dougalis, O. A. Karakashian, and W. R. McKinney. Fully-discrete methods with grid refinement for the generalized Korteweg-de Vries equation. *Viscous profiles and numerical methods for shock waves (Raleigh, NC, 1990)*, pages 1–11, 1990.
- [13] J. L. Bona, W. Pritchard, and L. R. Scott. A comparison of solutions of two model equations for long waves. Technical report, Wisconsin Univ-Madison Mathematics Research Center, 1983.
- [14] J. L. Bona, P. E. Souganidis, and W. A. Strauss. Stability and instability of solitary waves of Korteweg-de Vries type. *Proceedings of the Royal Society of London. A. Mathematical and Physical Sciences*, 411(1841):395–412, 1987.
- [15] J. C. Butcher. Implicit Runge-Kutta processes. *Mathematics of Computation*, 18(85):50–64, 1964.
- [16] J. Cai and J. Shen. Two classes of linearly implicit local energy-preserving approach for general multi-symplectic Hamiltonian PDEs. *Journal of Computational Physics*, 401:108975, 2020.

- [17] Y. Cheng and C.-W. Shu. A discontinuous Galerkin finite element method for time dependent partial differential equations with higher order derivatives. *Mathematics of Computation*, 77(262):699–730, 2008.
- [18] G. Cooper. Stability of Runge-Kutta methods for trajectory problems. *IMA journal of numerical analysis*, 7(1):1–13, 1987.
- [19] S. M. Cox and P. C. Matthews. Exponential time differencing for stiff systems. *J. Comput. Phys.*, 176(2):430–455, 2002.
- [20] W. Craig. An existence theory for water waves and the Boussinesq and Korteweg-de Vries scaling limits. *Communications in Partial Differential Equations*, 10(8):787–1003, 1985.
- [21] J. Cui, Y. Wang, and C. Jiang. Arbitrarily high-order structure-preserving schemes for the Gross-Pitaevskii equation with angular momentum rotation. *Computer Physics Communications*, 261:107767, 2021.
- [22] Y. Cui and D.-K. Mao. Numerical method satisfying the first two conservation laws for the Korteweg-de Vries equation. *Journal of Computational Physics*, 227(1):376–399, 2007.
- [23] V. A. Dougalis and O. A. Karakashian. On some high-order accurate fully discrete Galerkin methods for the Korteweg-de Vries equation. *Mathematics of Computation*, 45(172):329–345, 1985.
- [24] B. Fornberg and G. B. Whitham. A numerical and theoretical study of certain nonlinear wave phenomena. *Philosophical Transactions of the Royal Society of London. Series A, Mathematical and Physical Sciences*, 289(1361):373–404, 1978.
- [25] S. Geng. Construction of high order symplectic Runge-Kutta methods. *Journal of Computational Mathematics*, pages 250–260, 1993.
- [26] K. Goda. Numerical studies on recurrence of the Korteweg-de-Vries equation. *Journal of the Physical Society of Japan*, 42(3):1040–1046, 1977.
- [27] Y. Gong, J. Cai, and Y. Wang. Multi-symplectic fourier pseudospectral method for the Kawahara equation. *Communications in Computational Physics*, 16(1):35–55, 2014.
- [28] T. Grava and C. Klein. Numerical solution of the small dispersion limit of Korteweg-de Vries and Whitham equations. *Communications on Pure and Applied Mathematics: A Journal Issued by the Courant Institute of Mathematical Sciences*, 60(11):1623–1664, 2007.
- [29] T. Grava and C. Klein. A numerical study of the small dispersion limit of the Korteweg-de Vries equation and asymptotic solutions. *Physica D: Nonlinear Phenomena*, 241(23-24):2246–2264, 2012.
- [30] I. T. Greig and J. L. Morris. A hopscotch method for the Korteweg-de-Vries equation. *Journal of Computational Physics*, 20(1):64–80, 1976.
- [31] B.-Y. Guo and J. Shen. On spectral approximations using modified Legendre rational functions: application to the Korteweg-de-Vries equation on the half line. *Indiana University Mathematics Journal*, pages 181–204, 2001.
- [32] H. Holden, K. Karlsen, N. Risebro, and T. Tao. Operator splitting for the KdV equation. *Mathematics of Computation*, 80(274):821–846, 2011.
- [33] H. Holden, K. H. Karlsen, and N. H. Risebro. Operator splitting methods for generalized Korteweg-de-Vries equation. *Journal of Computational Physics*, 153(1):203–222, 1999.
- [34] W. Huang and D. M. Sloan. The pseudospectral method for third-order differential equations. *SIAM Journal on Numerical Analysis*, 29(6):1626–1647, 1992.
- [35] A. Jeffrey and T. Kakutani. Weak nonlinear dispersive waves: A discussion centered around the Korteweg-de Vries equation. *SIAM Review*, 14(4):582–643, 1972.
- [36] O. Karakashian and W. McKinney. On optimal high-order in time approximations for the Korteweg-de-Vries equation. *Mathematics of Computation*, pages 473–496, 1990.

- [37] A.-K. Kassam and L. N. Trefethen. Fourth-order time-stepping for stiff PDEs. *SIAM J. Sci. Comput.*, 26(4):1214–1233, 2005.
- [38] T. Kato. On the cauchy problem for the (generalized) Korteweg-de Vries equation. *Studies in Appl. Math. Adv. in Math. Suppl. Stud.*, 8:93–128, 1983.
- [39] C. E. Kenig, G. Ponce, and L. Vega. Well-posedness and scattering results for the generalized Korteweg-de Vries equation via the contraction principle. *Communications on Pure and Applied Mathematics*, 46(4):527–620, 1993.
- [40] C. Klein and J.-C. Saut. IST versus PDE, a comparative study, in Hamiltonian Partial Differential Equations and Applications. *Fields Institute Communications*, 75:383–449, 2015.
- [41] C. Klein and R. Peter. Numerical study of blow-up and dispersive shocks in solutions to generalized Korteweg-de Vries equations. *Phys. D*, 304/305:52–78, 2015.
- [42] P. D. Lax. Integrals of nonlinear equations of evolution and solitary waves. *Communications on Pure and Applied Mathematics*, 21(5):467–490, 1968.
- [43] J. Li and M. R. Visbal. High-order compact schemes for nonlinear dispersive waves. *Journal of Scientific Computing*, 26(1):1–23, 2006.
- [44] H. Liu and J. Yan. A local discontinuous Galerkin method for the Korteweg-de Vries equation with boundary effect. *Journal of Computational Physics*, 215(1):197–218, 2006.
- [45] H. Liu and N. Yi. A Hamiltonian preserving discontinuous Galerkin method for the generalized Korteweg-de Vries equation. *Journal of Computational Physics*, 321:776–796, 2016.
- [46] Z. Liu, H. Zhang, X. Qian, and S. Song. Mass and energy conservative high order diagonally implicit Runge-Kutta schemes for nonlinear Schrödinger equation in one and two dimensions. *arXiv preprint arXiv:1910.13700*, 2019.
- [47] H. Ma and W. Sun. A Legendre–Petrov–Galerkin and Chebyshev collocation method for third-order differential equations. *SIAM Journal on Numerical Analysis*, 38(5):1425–1438, 2000.
- [48] H. Ma and W. Sun. Optimal error estimates of the Legendre–Petrov–Galerkin method for the Korteweg-de Vries equation. *SIAM Journal on Numerical Analysis*, 39(4):1380–1394, 2001.
- [49] Y. Martel and F. Merle. Instability of solitons for the critical generalized Korteweg—de Vries equation. *Geometric & Functional Analysis GAFA*, 11(1):74–123, 2001.
- [50] Y. Martel and F. Merle. Stability of blow-up profile and lower bounds for blow-up rate for the critical generalized KdV equation. *Annals of mathematics*, pages 235–280, 2002.
- [51] Y. Martel and F. Merle. Asymptotic stability of solitons of the gKdV equations with general nonlinearity. *Mathematische Annalen*, 341(2):391–427, 2008.
- [52] Y. Martel, F. Merle, et al. Nonexistence of blow-up solution with minimal L2-mass for the critical gKdV equation. *Duke Mathematical Journal*, 115(2):385–408, 2002.
- [53] Y. Martel, F. Merle, and P. Raphaël. Blow up for the critical generalized Korteweg-de Vries equation. i: Dynamics near the soliton. *Acta Mathematica*, 212(1):59–140, 2014.
- [54] F. Merle. Existence of blow-up solutions in the energy space for the critical generalized KdV equation. *Journal of the American Mathematical Society*, 14(3):555–578, 2001.
- [55] R. M. Miura, C. S. Gardner, and M. D. Kruskal. Korteweg-de Vries equation and generalizations. II. Existence of conservation laws and constants of motion. *Journal of Mathematical Physics*, 9(8):1204–1209, 1968.
- [56] J. Sanz-Serna. Runge-Kutta schemes for Hamiltonian systems. *BIT Numerical Mathematics*, 28(4):877–883, 1988.
- [57] J. Sanz-Serna and L. Abia. Order conditions for canonical Runge-Kutta schemes. *SIAM Journal on Numerical Analysis*, 28(4):1081–1096, 1991.

- [58] G. Schneider and C. E. Wayne. On the validity of 2d-surface water wave models. *GAMM Mitt. Ges. Angew. Math. Mech*, 25(1-2):127–151, 2002.
- [59] A. C. Scott, F. Y. F. Chu, and D. W. McLaughlin. The soliton: A new concept in applied science. *Proceedings of the IEEE*, 61(10):1443–1483, 1973.
- [60] J. Shen. A new dual-Petrov-Galerkin method for third and higher odd-order differential equations: application to the KdV equation. *SIAM Journal on Numerical Analysis*, 41(5):1595–1619, 2003.
- [61] J. Shen, T. Tang, and L.-L. Wang. *Spectral methods*, volume 41 of *Springer Series in Computational Mathematics*. Springer, Heidelberg, 2011. Algorithms, analysis and applications.
- [62] J. Shen and J. Xu. Convergence and error analysis for the scalar auxiliary variable (SAV) schemes to gradient flows. *SIAM Journal on Numerical Analysis*, 56(5):2895–2912, 2018.
- [63] J. Shen, J. Xu, and J. Yang. The scalar auxiliary variable (SAV) approach for gradient flows. *Journal of Computational Physics*, 353:407–416, 2018.
- [64] J. Shen, J. Xu, and J. Yang. A new class of efficient and robust energy stable schemes for gradient flows. *SIAM Review*, 61(3):474–506, 2019.
- [65] L. N. Trefethen. *Spectral methods in MATLAB*, volume 10 of *Software, Environments, and Tools*. Society for Industrial and Applied Mathematics (SIAM), Philadelphia, PA, 2000.
- [66] A. Vliegthart. On finite-difference methods for the Korteweg-de-Vries equation. *Journal of Engineering Mathematics*, 5(2):137–155, 1971.
- [67] R. Winther. A conservative finite element method for the Korteweg-de-Vries equation. *Mathematics of Computation*, pages 23–43, 1980.
- [68] Y. Xu and C.-W. Shu. Error estimates of the semi-discrete local discontinuous Galerkin method for nonlinear convection–diffusion and KdV equations. *Computer methods in applied mechanics and engineering*, 196(37-40):3805–3822, 2007.
- [69] J. Yan and C.-W. Shu. A local discontinuous Galerkin method for kdv type equations. *SIAM Journal on Numerical Analysis*, 40(2):769–791, 2002.
- [70] N. Yi, Y. Huang, and H. Liu. A direct discontinuous Galerkin method for the generalized Korteweg-de Vries equation: energy conservation and boundary effect. *Journal of Computational Physics*, 242:351–366, 2013.
- [71] N. J. Zabusky and M. D. Kruskal. Interaction of "solitons" in a collisionless plasma and the recurrence of initial states. *Phys. Rev. Lett.*, 15:240–243, Aug 1965.